Journal of Power Sources Advances 9 (2021) 100056

Contents lists available at ScienceDirect

Journal of Power Sources Advances

journal homepage: www.journals.elsevier.com/journal-of-power-sources-advances

Determination of state-of-charge dependent diffusion coefficients and kinetic rate constants of phase changing electrode materials using physics-based models

Kudakwashe Chayambuka [a,b,c], Grietus Mulder [b,c], Dmitri L. Danilov [a,d], Peter H.L. Notten [a,d,e,*]

[a] Eindhoven University of Technology, P.O. Box 513, 5600, MB Eindhoven, the Netherlands
[b] VITO, Boeretang 200, 2400, Mol, Belgium
[c] EnergyVille, Thor Park 8310, 3600, Genk, Belgium
[d] Forschungszentrum Jülich, Fundamental Electrochemistry (IEK-9), D-52425 Jülich, Germany
[e] Centre for Clean Energy Technology, University of Technology Sydney, Broadway, Sydney, NSW, 2007, Australia

ARTICLE INFO

Keywords:
Batteries
P2D
modeling
sodium-ion
GITT

ABSTRACT

The simplified gravimetric intermittent titration technique (GITT) model, which was first proposed by Weppner and Huggins in 1977, remains a popular method to determine the solid-state diffusion coefficient (D_1) and the electrochemical kinetic rate constant (k). This is despite the model having been developed on the premise of a single-slab electrode and other gross simplification which are not applicable to modern-day porous battery electrodes. Recently however, more realistic and conceptually descriptive models have emerged, which make use of the increased availability of computational power. Chief among them is the P2D model developed by Newman et al., which has been validated for various porous battery electrodes. Herein, a P2D GITT model is presented and coupled with grid search optimization to determine state-of-charge (SOC) dependent D_1 and k parameters for a sodium-ion battery (SIB) cathode. Using this approach, experimental GITT steps could be well fitted and thus validated at different SOC points. This work demonstrates the first usage of the P2D GITT model coupled with optimization as an analytical method to derive and validate physically meaningful parameters. The accurate knowledge of D_1 and k as a function of the SOC gives further insight into the SIB intercalation dynamics and rate capability.

1. Introduction

Understanding internal battery dynamics, in particular, the charge transport mechanisms in porous electrodes, is fundamental for building better batteries. Within lithium-ion battery (LIB) and sodium-ion battery (SIB) electrodes, solid-state diffusion is usually the slowest and thus the rate-determining process. Knowledge of the solid-state diffusion coefficient (D_1) and kinetic rate constant (k) is therefore fundamental in designing battery electrodes for optimized power and energy efficiency. As a result, it is important to develop experimentally accurate and validated characterization methods, to determine solid-state mass transport parameters.

State-of-the-art electroanalytical techniques, to determine D_1 in battery electrodes include: slow scan rate cyclic voltammetry (SSCV) [1], electrochemical impedance spectroscopy (EIS) [2], potentiostatic intermittent titration technique (PITT) [3–7], and gravimetric intermittent titration technique (GITT) [8,9]. These techniques generally consist of displacing the electrochemical system from a state of equilibrium by imposing a step, in either constant voltage (CV) or constant current (CC), while simultaneously measuring the other (dependent) variable as a function of time [10]. D_1 and k parameters determined by each of the aforementioned electroanalytical techniques are known to vary by orders of magnitude [2,6,11]. This is primarily because of the different time scales at which the techniques are accurate and the simplified analytical methods used to derive the parameters, which are inconsistent with the underlying phenomena and experimental conditions.

The most common electroanalytical technique for determining electrode D_1 and k parameters is the GITT method, which was first proposed by Weppner and Huggins in 1977 [8]. The GITT technique starts with a cell in which electrodes are in equilibrium. A galvanostatic, *i.e.,* CC pulse is then applied for a short period of time, while the system voltage response is measured as a function of time. After the CC period, the cell is

* Corresponding author. Eindhoven University of Technology, P.O. Box 513, 5600, MB Eindhoven, the Netherlands.
E-mail address: p.h.l.notten@tue.nl (P.H.L. Notten).

https://doi.org/10.1016/j.powera.2021.100056
Received 29 January 2021; Received in revised form 1 April 2021; Accepted 21 April 2021

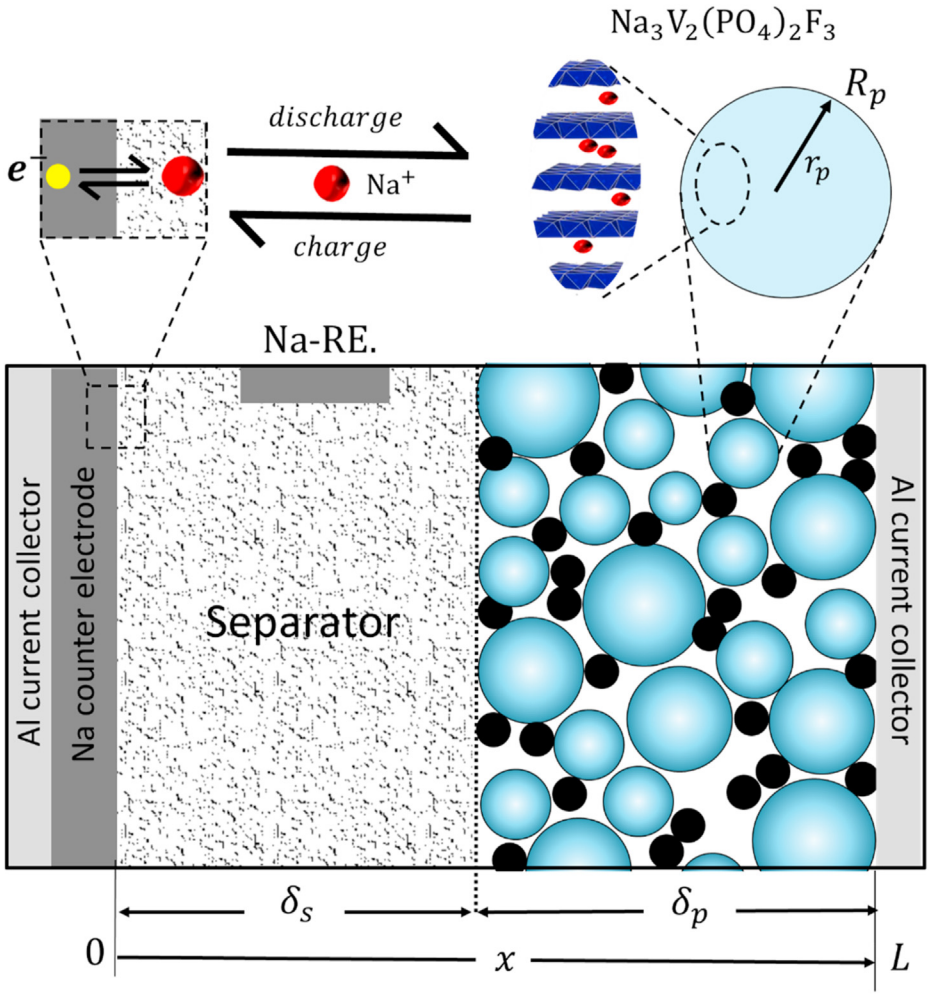

Fig. 1. Three electrode half-cell setup used in GITT experiments. The blue circles represent the NVPF active electrode material, and the black circles represent the carbon-based conductive filler. At the particle scale and at the electrode interface, the charge insertion mechanisms are shown. The red and yellow spheres represent sodium cations and electrons, respectively. (For interpretation of the references to colour in this figure legend, the reader is referred to the Web version of this article.)

then set in open-circuit voltage (OCV) mode, and the relaxation voltage profile is recorded. The OCV of the cell approaches the equilibrium voltage in the long run. Ideally, the GITT procedure is performed in a three-electrode half-cell configuration wherein the working electrode (WE) is composed of the electrode material under investigation, a metallic counter electrode (CE) and a reference electrode (RE) of the first kind. Fig. 1 illustrates a three-electrode SIB half-cell configuration for GITT measurements, composed of $Na_3V_2(PO_4)_2F_3$ (NVPF) as WE and metallic Na as CE and RE (Na-RE).

In developing an analytical model for GITT measurements, Weppener et al. introduced several simplifying assumptions regarding electrochemical charge transport pathways and system dimensions. These include [7,12]:

(i) Diffusion occurs across a 1-dimensional plane of a dense electrode geometry.
(ii) Diffusion in the electrode is governed by Fick's laws and occurs within a very thin film close to the electrode/electrolyte interface (this assumes a semi-infinite medium).
(iii) Concentration profiles in the electrolyte are considered negligible.
(iv) The diffusion coefficient remains constant during a single pulse and subsequent relaxation period.
(v) There are no phase transformation effects on the electrode diffusion and kinetics.
(vi) Volume and porosity changes are negligible.
(vii) Overpotentials in the electrolyte and at electrode/electrolyte interface are negligible.
(viii) The electrochemical double-layer capacitance is ignored.

Based on these assumptions, the analytical expression for the diffusion coefficient following a galvanostatic GITT perturbation is expressed as [13].

$$D_1 = \frac{4}{\pi\tau}\left(\frac{I\,V_m}{FA}\right)^2\left(\frac{dU/dy}{dV\Big/d\sqrt{\tau}}\right)^2,\ \forall\,\tau \ll L^2\Big/D_1 \tag{1}$$

where D_1 is the diffusion coefficient of the material [$m^2\ s^{-1}$], I the current during the GITT CC pulse [A], V_m the molar volume of the active material [$m^3\ mol^{-1}$], F the Faraday's constant 95485 [$C\ mol^{-1}$], A the porous electrode active surface area [m^2], U and V are the electrode equilibrium potential and electrode potential during the CC pulse, respectively [V], τ the CC pulse duration [s], y the electrode state-of-charge (SOC) based on stoichiometry [−] and L the thickness of the active material [m]. The limiting condition for τ, *i.e.*, $\tau \ll L^2/D$, is necessary to satisfy the boundary conditions and the assumptions (i) and (ii) above.

Using porous battery electrodes, it is practically impossible to create conditions to satisfy the fundamental assumptions for Eq. (1). This is because porous battery electrodes are composed of a mixture of

Table 1
Summary of equations used in the P2D GITT model.

Model	Expression	Eq.	Boundary conditions
NVPF (positive) electrode $\delta_s \le x \le L$			
Mass balance in electrolyte	$\frac{\partial c_2}{\partial t} = \frac{\partial}{\partial x}\left(D_{2,p}^{eff}\frac{\partial c_2}{\partial x}\right) + (1 - t_+)a_p j_p$	(2)	$\frac{\partial c_2}{\partial x}\Big\|_{x=L} = 0$
Potential in electrolyte	$i_{2,p} = -\kappa_p^{\text{eff}}\frac{\partial \varphi_{2,p}}{\partial x} + \frac{\kappa_p^{\text{eff}} RT}{F}(1-2t_+)\cdot\nabla \ln c_2$	(3)	
Potential in solid	$i_{1,p} = -\sigma_p^{eff}\frac{\partial \varphi_{1,p}}{\partial x}$	(4)	
Charge conservation	$i_{tot} = i_{1,p} + i_{2,p},$	(5)	
Surface flux	$a_p j_p F = \frac{\partial i_{2,p}}{\partial x}$	(6)	$i_{2,p}\Big\|_{x=\delta_s} = i_{tot}$ $i_{2,p}\Big\|_{x=L} = 0$
Electrode kinetics	$j_p = j_{0,p}\left[\frac{c_{1,p}^s}{\bar{c}_{1,p}}\exp\left(\frac{\alpha F}{RT}\eta_p^{ct}\right) - \frac{c_{1,p}^{\max} - c_{1,p}^s}{c_{1,p}^{\max} - \bar{c}_{1,p}}\frac{c_2}{\bar{c}_2}\exp\left(-\frac{(1-\alpha)F}{RT}\eta_p^{ct}\right)\right]$	(7)	
Exchange current	$j_{0,p} = F k_p (c_{1,p}^{max} - \bar{c}_{1,p})^{\alpha_a}(\bar{c}_2)^{\alpha_a}(\bar{c}_{1,p})^{\alpha_c}$	(8)	
Overpotential	$\eta_m^{ct} = \varphi_{1,p} - \varphi_{2,p} - U_p(c_{1,p}^s, T)$	(9)	
Fick's second law	$\frac{\partial c_{1,p}}{\partial t} = \frac{1}{r_p^2}\frac{\partial}{\partial r_p}\left(D_{1,p} r_p^2 \frac{\partial c_{1,p}}{\partial r_p}\right)$	(10)	$\frac{\partial c_{1,p}}{\partial r_p}\Big\|_{r=0} = 0$ $-D_{1,p}\frac{\partial c_{1,p}}{\partial r_p}\Big\|_{r_p=R_p} = j_p$
Separator (dilute solution theory) $0 \le x \le \delta_s$			
Potential distribution	$i_{tot} = i_{2,s} = -\kappa_s^{\text{eff}}\frac{\partial \varphi_{2,s}}{\partial x} + \frac{\kappa_s^{\text{eff}} RT}{F}(1-2t_+)\cdot\nabla \ln c_2$	(11)	$\varphi_{2,s}\Big\|_{x=0} = 0$
Fick's second law	$\frac{\partial c_2}{\partial t} = \frac{\partial}{\partial x}\left(D_{2,s}^{eff}\frac{\partial c_2}{\partial x}\right)$	(12)	$\frac{\partial c_2}{\partial x}\Big\|_{x=0} = -\frac{i_{tot}(1-t_+)}{F D_{2,s}^{eff}}$
Battery voltage			
RE Potential	$\varphi_{1,ref} = \frac{RT}{F}\ln(c_2\|_{x=0})$	(13)	
Battery voltage	$V_{bat} = \varphi_{1,p}\|_{x=L} - \varphi_{1,ref}$	(14)	

spherical, micron-sized active particles and a liquid electrolyte. This fundamentally differs from the description of a monolithic phase or "single-slab" active material used to derive Eq. (1). In addition, it has proved difficult to confidently determine the A and V_m parameters [14,15]. Moreover, the diffusion time constant in spherical particles of radius $L: \tau' = L^2/4D_1$ is, in fact, four times less than $\tau = L^2/D_1$, the diffusion time constant in a 1-dimensional plane of thickness L. As a result, mass transport in spherical active particles, cannot be assumed to occur exclusively within a thin interfacial layer. Finally, concentration profiles across the entire electrode thickness and electrolyte should not be overlooked. While there have been notable efforts to derive analytical GITT solutions for porous battery electrodes [16], it is scientifically prudent to forego the simplifying assumptions and determine k and D_1 parameters, based on numerical models.

The application of numerical, physics-based pseudo-two-dimensional (P2D) models to analyze GITT dates back to 2009 [12,17–19]. P2D models use coupled, non-linear partial differential equations to describe mass transport and kinetics in porous battery electrodes. Dees et al. [12] developed a P2D model to analyze GITT experimental data of a Li/ / $LiNi_{0.8}Co_{0.15}Al_{0.05}O_2$. Bernardi et al. [19] similarly applied a P2D model built in COMSOL Multiphysics®. In general, the P2D GITT models predictions show reasonable agreement with experimental data. These pioneering works demonstrate the utility of physics-based models as

Table 2
Physical and electrochemical properties of the Na//NVPF half-cell.

Parameter	Unit	Description	Value	Reference
Physical properties				
δ_s	μm	Separator thickness	220	El cell
δ_p	μm	NVPF positive electrode thickness	68	measured
R_p	μm	The radius of NVPF particles	0.69	measured
A	cm^2	Electrode geometric surface area	2.545	measured
ε_p^e	–	Electrode porosity	0.23	optimized
ε_p^f	–	Binder and conductive filler fraction	0.22	optimized
ε_s^e	–	Separator porosity	0.95	El cell
ρ_p	g cm^{-3}	Density of NVPF	3.2	[23]
NVPF porous electrode properties				
$c_{1,p}^{max}$	mol l^{-1}	Maximum concentration	12.00	measured
$c_{1,p}^{min}$	mol l^{-1}	Minimum concentration	3.319	measured
$C_{1,p}^{rev}$	mAh g^{-1}	Reversible electrode capacity	100.5	measured
σ_p^{eff}	S m^{-1}	Electrode electric conductivity	50	estimated
Electrolyte properties				
$c_2(t=0)$	mol kg^{-1}	Initial electrolyte concentration	1.0	measured
D_2	$m^2 s^{-1}$	Diffusion coefficient	$4.46 \cdot 10^{-12}$	AEM
κ	S m^{-1}	ionic conductivity	1.0	AEM
t_+	–	Transference number	0.45	AEM

GITT analytical tools. Nevertheless, the P2D GITT models lacked a parameter optimization strategy and they were only applied on a few selected points across the full SOC range. Surprisingly, however, the increased adoption of P2D GITT models in more recent studies has been underwhelming.

In this work, a MATLAB® based P2D GITT model coupled with grid search optimization is used as a strategy to derive SOC dependent D_1 and k parameters. A three-electrode SIB half-cell based on an NVPF cathode/positive electrode, a Na CE, and a Na-RE is used to determine the GITT experimental data. To realize P2D GITT models' full potential, they must be available in openly accessible environments [20]. In addition, the models should be equipped with optimization strategies to determine the unknown parameters at different SOC points. This is crucial for understanding phase transformations. Because of the high accuracy, experimental validation, and ease of parameter optimization, the P2D GITT model is a recommended analytical GITT method.

2. Experimental

PAT-Cells (EL-Cell GmbH, Hamburg, Germany) were used as electrochemical test cells. A PAT-Cell is composed of an 18 mm diameter PAT-core, in which battery electrodes can be assembled. Components of the PAT-core include a factory-built separator (FS–5P, Freudenberg Viledon FS 2226E + Lydall Solupor 5P09B) and a preassembled Na-RE (See Supplementary Fig. 1).

Na and NVPF electrodes were thus assembled into a SIB half-cell configuration, in which an electrolyte composed of 1 M $NaPF_6$ dissolved in ethylene carbonate (EC) and propylene carbonate (PC), $EC_{0.5}$: $PC_{0.5}$ (w/w) was used. The NVPF electrodes used were produced during the EU-funded NAIADES project and were supplied by the manufacturer (SAFT/CEA) [21,22]. These had a single-side average coating thickness of 68 μm, which was measured by a digital-micrometer screw gauge (Helios Preisser, Digi-Met) and a mass loadings of 12 mg cm^{-2} [23]. Based on scanning electron microscopy (SEM) micrographs obtained on Quanta FEG 650 (FEI, USA), the particle size distribution and the average particle size were determined (See Supplementary Fig. 2).

After assembly in an argon-filled glove box, the PAT-Cells were her-

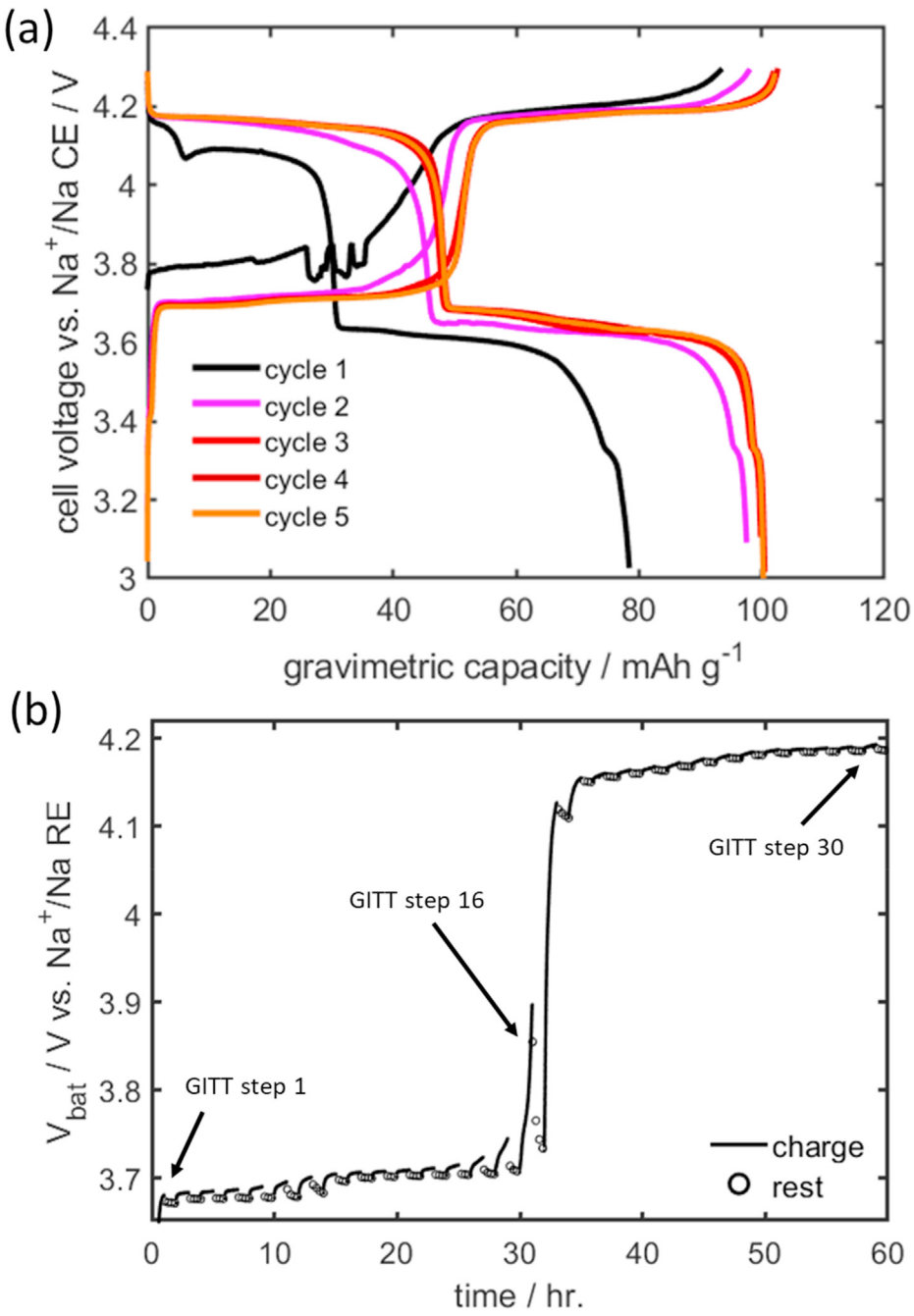

Fig. 2. Experimental results obtained for the Na//NVPF SIB half-cell. Formation cycles recorded at a CC of 0.1 mA (0.039 $mA\ cm^{-2}$, C/30) (a). Overview of 30 GITT steps during (de)sodiation (solid lines) at a CC of 0.1 mA and OCV rest periods (circles) (b). All measured 30 GITT steps are shown.

metically sealed and placed in a climate chamber at 25 °C. GITT was performed on the half-cells at 25 °C. Cell voltage measurements were recorded using a Maccor® automated cycling equipment (Model 4200). The cells initially underwent five formation cycles at a CC of 0.1 mA (0.039 mA cm^{-2}, C/30) and a reversible electrode capacity of 3.1 mAh was obtained in the cell voltage range of 3.0–4.3 V. After the formation stage, the cells were discharged to 3.0 V in the CV mode for 3 h to ensure a fully discharged starting point for the GITT cycles.

30 GITT steps, comprised of a CC charge of 0.1 mA until the cell capacity reached 0.1 mAh followed by an OCV relaxation for 1 h, were applied. Because Coulomb counting was used to define the pulse breaks (and not time), the total pulse duration was approximately 1 h. A low charging current was applied to avoid high overpotentials and multiple parameter sensitivity. Besides, a long pulse duration is necessary to eliminate the double-layer capacitance effects, which are not included in the present P2D model. Therefore, based on these experimental conditions, only the equilibrium potential, the kinetic rate constant, and the solid-state diffusion coefficient are the sensitive parameters to the model voltage response.

2.1. Model

A P2D GITT model consisting of a set of coupled partial differential equations is coded in MATLAB. The model considered a CC pulse of $i_{tot} =$ 0.039 mA cm^{-2} (C/30) applied for 1 h, followed by an OCV relaxation for 1 h.

Table 1 summarizes the set of equations used in the half-cell model. The equations and boundary conditions were discretized using backward

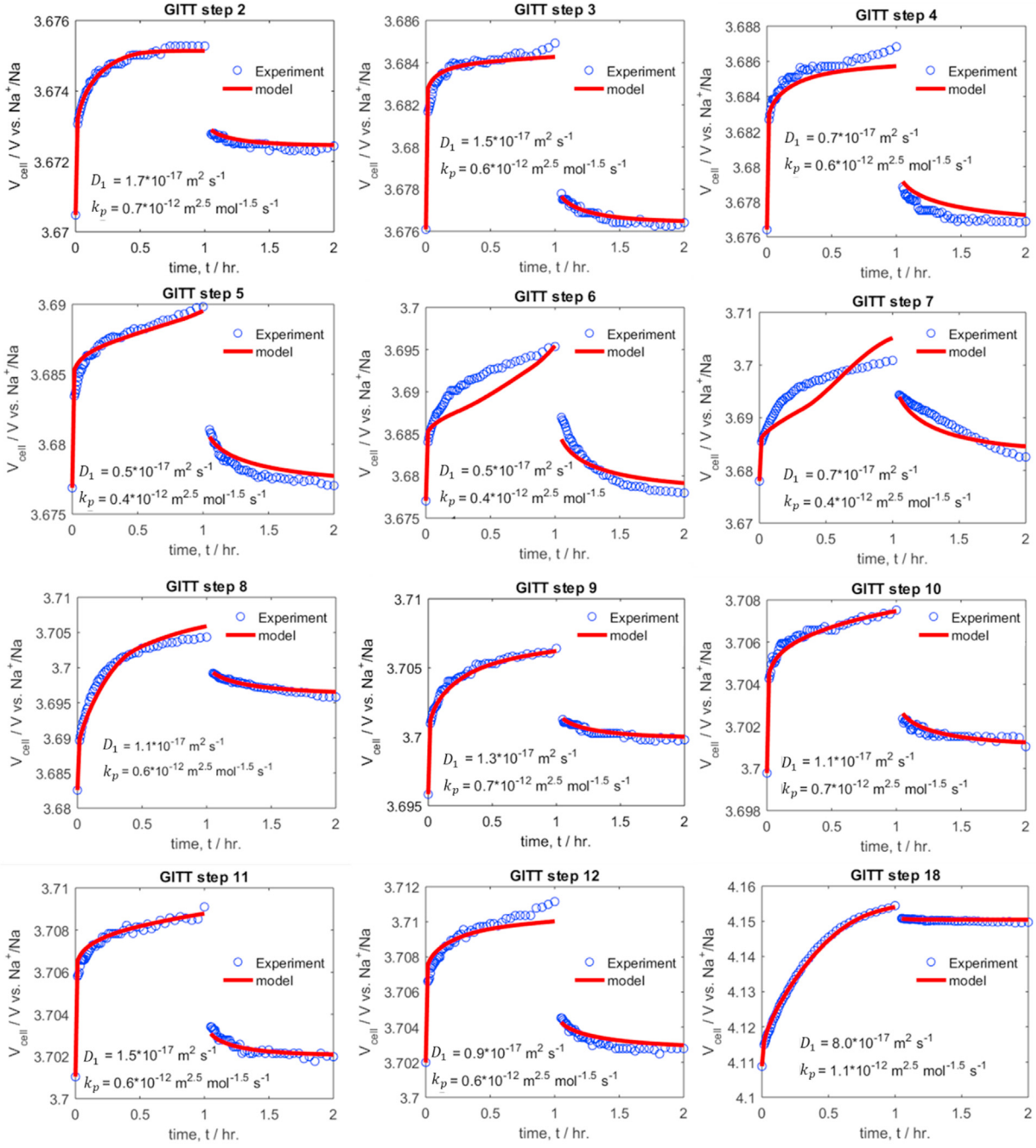

Fig. 3. Experimental (symbols) and modeled (lines) voltages and optimized diffusion coefficients and kinetic rate constants for GITT steps 2–18.

and forward difference schemes. Variables *c*, *φ*, *and i* describe the concentration, electric potential, and current, respectively. Subscripts 1 and 2 in the variable symbols represent the phase in which the variable is defined, where 1 and 2 represent the solid and the liquid electrolyte phase, respectively. Subscripts *p* and *s* represent the domain/region in which the variable is defined, where *p* and *s* represent the positive electrode and separator regions, respectively. In the P2D model, a distinction is thus made between electronic current density in the positive electrode ($i_{1,p}$) and ionic current density ($i_{2,p}$). Both $i_{1,p}$ and $i_{2,p}$ add up to the total applied current density (i_{tot}) by charge conservation. Similarly, $\varphi_{1,p}$ and $\varphi_{2,p}$ represent the potential in the solid and electrolyte phase, respectively.

In the NVPF active particles, mass transport is described by Fick's second law, which determines the concentration $c_{1,p}$ and the average concentration $\bar{c}_{1,p}$ in time. Analytical and numerical methods can be applied to solve the solid-state diffusion problem with Neumann flux boundary conditions [24]. In this model, the hybrid backward Euler control volume method is used [25]. The NVPF electrode equilibrium potential U_p is further determined by linear interpolation between two successive GITT relaxation endpoints.

The porous electrode surface area per unit volume a_p [m^{-1}] is calculated as

$$a_p = \frac{3\left(1-\varepsilon_p^e-\varepsilon_p^f\right)}{R_p} \tag{15}$$

where R_p is the mean radius of the NVPF active particles [*m*] and ε_p^e and ε_p^f are the electrolyte and additive filler volume fractions, respectively [−].

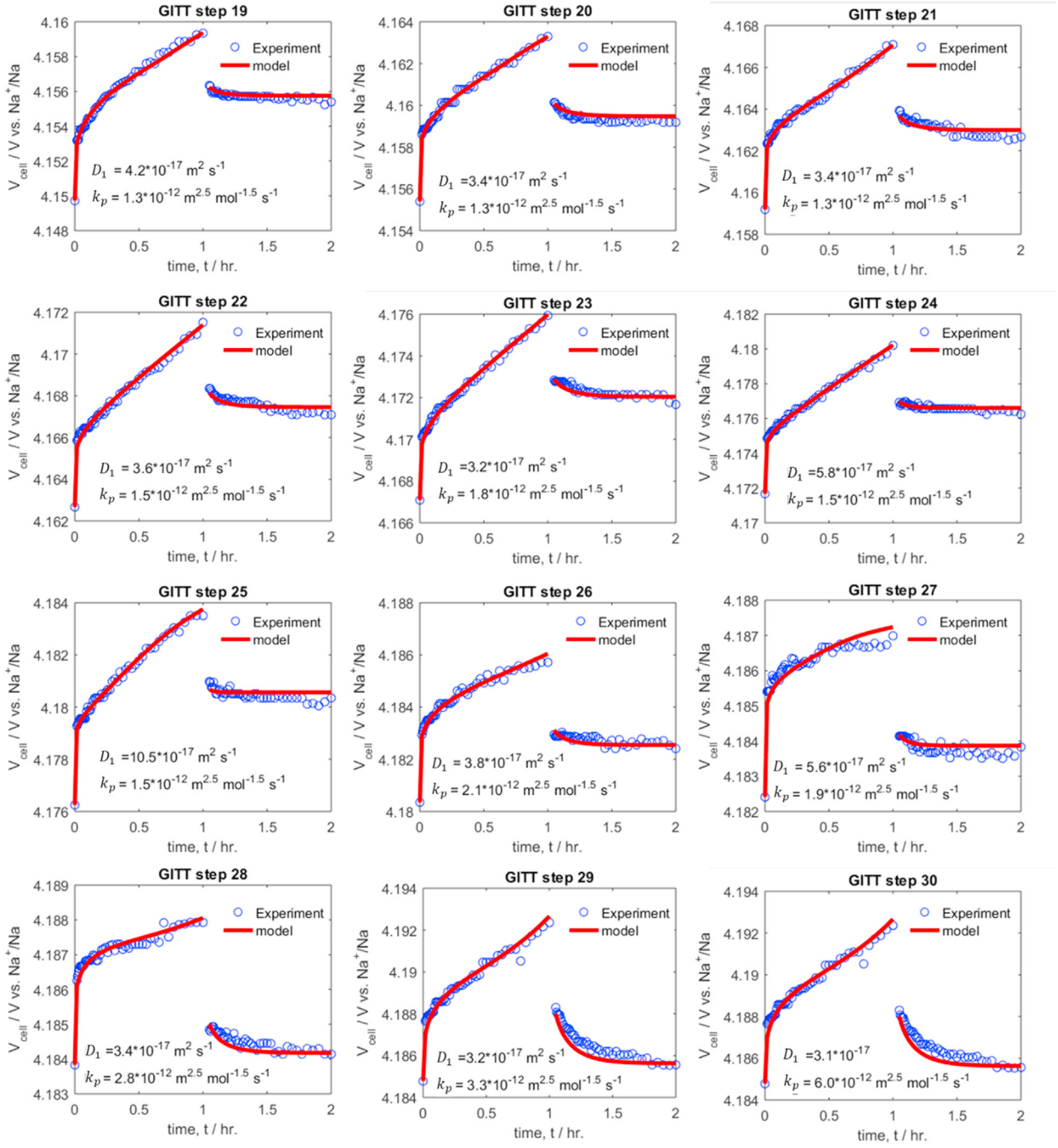

Fig. 4. Experimental (symbols) and modeled (lines) voltages, and optimized diffusion coefficients and kinetic rate constants for GITT steps 19–30.

ε_p^f includes volume fractions the binder and carbon conductive filler, the non-active constituents of the NVPF electrode.

The GITT cell voltage (V_{bat}) is finally calculated from the difference between the NVPF electrode potential and the RE potential ($\varphi_{1,ref}$) [V]. The advantage of the Na-RE is that it does not introduce additional unknown parameters of the kinetics of the Na^+/Na CE to the model. This property is convenient in limiting the number of unknowns.

Table 2lists the parameters for the three-electrode half-cell used in the P2D GITT model. Electrode parameters were either measured, optimized, or taken from literature. Separator properties were obtained from the manufacturer (EL Cell). The electrolyte properties were model-derived using the advanced electrolyte model (AEM) version. 2.19.1 [26].

The initial particles' SOC for each GITT step is calculated based on the electrode average cumulative capacity, which is updated after each step. The only unknown parameters are, therefore, $D_{1,p}$ the solid-state diffusion coefficient in NVPF particles [$m^2\ s^{-1}$] and k_p the kinetic rate constant in NVPF [$m^{2.5}\ mol^{-1.5}s^{-1}$]. First, a range of expected values is determined. This is achieved by 'trial and error' to determine the upper and lower parameter boundaries. Then a set of evenly spaced values is selected from this range. By taking all pair combinations of $D_{1,p}$ and k_p and calculating the least-squared difference between experimental and model cell voltage (V_{cell}), a 2-dimensional grid of the least-squared difference is obtained. The optimum $D_{1,p}$ and k_p combination is then determined from the global minimum on this grid. This procedure is repeated for each GITT step. The estimation error range is finally determined from the range of $D_{1,p}$ and k_p combinations which result in 10%

variation from the optimum combination. Because the model can run fast, approximately 2 s for each GITT charge and relaxation, optimized results can be obtained in a reasonable time. An animation of a P2D GITT model results is shown in supplementary files.

3. Results and discussion

Fig. 2a shows the 5 initial formation cycles recorded for the Na// NVPF half-cell. A reversible gravimetric capacity of 101 mAh g^{-1} is obtained after 5 cycles. Fig. 2b shows the experimental results of 30 GITT steps obtained. The NVPF electrode shows voltage plateaus and steep steps, the characteristic features of phase changes in the electrode material. From the raw experimental data, evidence of $D_{1,p}$ variations can be observed from the changes in OCV relaxation profiles, as a function of SOC. In addition, phase transition regions also result in slow OCV relaxation. The application of the P2D model and the grid search optimization can nevertheless determine $D_{1,p}$ and k_p parameters as a function of SOC.

Fig. 3 and Fig. 4 show the experimental (blue symbols) and optimized model results (red curves) for 24 of the 30 GITT steps. The P2D model predicts well both the CC charging and OCV relaxation stages by optimizing $D_{1,p}$ and k_p parameters. It is worth highlighting that in the CC stage, both $D_{1,p}$ and k_p are sensitive, while in the relaxation step, only $D_{1,p}$ is sensitive. Comparing the model voltage profiles at different SOC, it can be concluded that the model accuracy is higher in the voltage plateau regions than in voltage sloping regions. This is because of two main reasons: first, U_p is accurately deduced in the plateau regions, from linear interpolation of successive GITT relaxation endpoints. Second, phase changes in the material do not occur instantaneously. Therefore, the model assumption of solid-solution intercalation with a constant $D_{1,p}$ (over each GITT step), remains valid.

A plot of $D_{1,p}$ and k_p parameters as a function of SOC is shown in Supplementary Fig. 3. $D_{1,p}$ values show spikes at the NVPF steep voltage step points. In addition, moving from the low voltage GITT steps (step 1 to 16) to the high voltage GITT steps (step 17 to 30), $D_{1,p}$ values show a clear shift in their order of magnitude. Correlating the changes in $D_{1,p}$ to the NVPF phase changes, can be further verified using *in-operando* synchrotron-based scanning transmission x-ray microscopy [27]. On the other hand, k_p values exponentially increase as the SOC increases, indicating faster electrode kinetics at lower Na^+ concentrations in the NVPF active particles. These results will be used in future works as input parameters in the modeling of full cell SIBs.

However, not all GITT steps could be accurately modeled by the P2D model, particularly steps 6 and 7 and the steep voltage region around GITT step 16 (see Fig. 2). This is because phase separations and EMF voltage hysteresis occur in these regions. These 'non-ideal' effects induce additional overpotentials which are not presently captured by the solid-solution model. One can include in the model the intercalation dynamics of multiphase materials and moving boundary phase field models to address this shortcoming [6,28–31]. Detailed comparisons with such models will be the subject of future works.

A comparison of the P2D GITT model results with two analytical model results is shown in Supplementary Fig. 4. The first analytical result is based on literature results by Liu et al. [32], while the second is based on the Weppner model [33] applied to the GITT data herein obtained. Both the P2D GITT and the Weppner model show results in the same order of magnitude. However, results from Liu et al. [32] are approximately 6 orders of magnitude higher, showing clear deviation. Although the reasons for such a difference are not yet clear, such a high value in $D_{1,p}$ is unusual in electrode materials. Nevertheless, none of the analytical methods show $D_{1,p}$ profiles which are consistent with phase changes in the NVPF electrode.

4. Conclusions

A P2D GITT model has been used as an analytical tool to simultaneously determine D_1 and k parameters at different electrode SOC. The P2D GITT model herein shown accurately simulates the experimental voltage profiles of an NVPF SIB half-cell. Better model agreement is observed in the voltage plateau regions because of the absence of phase transitions. In these regions, the assumption of the solid-solution intercalation mechanism is valid.

P2D models are often criticized for the large number of parameters used. However, in half-cell configurations and using a RE, the number of parameters is drastically reduced. The low constant current pulses used in GITT experiments ensure that other electrochemical parameters are not sensitive and therefore do not need to be conjointly optimized (as long as they fall within a reasonable range). As a result, the P2D GITT model can be optimized by two parameters only.

The advantages of the P2D GITT model over the classical analytical models originate from the replacement of unrealistic model assumptions with an accurate porous electrode description. Furthermore, GITT current pulses can be longer and are not restricted by the $\tau \ll L^2/D$ condition. This means experimental runtimes can be shortened. Moreover, two key battery modeling parameters are obtained from one set of GITT data. Finally, parameter estimates are immediately validated by the quality of the model fit compared to experimental GITT profiles. This is not the case in any of the analytical models. For physics-based modeling, it is also advantageous for D_1 and k parameters to be determined by the same model, instead of relying on two different techniques with, as we have seen, different assumptions.

The methods herein elaborated have been introduced for the SIB system but can be applied to any porous battery electrode material to yield similar results. The (dis)charge performance of intercalation electrode materials is mainly attributed to solid-state mass transport, the knowledge of D_1 and k can be readily incorporated in electrode design, physics-based modeling, and benchmarking tools. This information will be used in forthcoming publications to model the NVPF electrode performance at various (dis)charge rates, further explore intercalation-induced phase changes in the NVPF material with operando techniques, and better understand the multiphase intercalation dynamics in this electrode material.

Acknowledgements

D.L.D. has received funding from the European Union's Horizon 2020 Research and Innovation Program under Grant Agreement No. 769900-DEMOBASE. K.C. and G.M. are grateful for the support from the European Union's Horizon 2020 Research and Innovation Program under Grant Agreement No. 646433-NAIADES.

Appendix A. Supplementary data

Supplementary data to this article can be found online at https://doi.org/10.1016/j.powera.2021.100056.

Declaration of interests

The authors declare that they have no known competing financial interests or personal relationships that could have appeared to influence the work reported in this paper.

References

[1] D. Aurbach, M.D. Levi, E. Levi, H. Teller, B. Markovsky, G. Salitra, U. Heider, L. Heider, Common electroanalytical behavior of Li intercalation processes into graphite and transition metal oxides, J. Electrochem. Soc. 145 (1998) 3024, https://doi.org/10.1149/1.1838758.

[2] D.R. Baker, C. Li, M.W. Verbrugge, Similarities and differences between potential-step and impedance methods for determining diffusion coefficients of lithium in

active electrode materials, J. Electrochem. Soc. 160 (2013) A1794, https://doi.org/10.1149/2.076310jes.
[3] M.D. Levi, D. Aurbach, Diffusion coefficients of lithium ions during intercalation into graphite derived from the simultaneous measurements and modeling of electrochemical impedance and potentiostatic intermittent titration characteristics of thin graphite electrodes, J. Phys. Chem. B 101 (1997) 4641–4647, https://doi.org/10.1021/jp9701911.
[4] S. Malifarge, B. Delobel, C. Delacourt, Guidelines for the analysis of data from the potentiostatic intermittent titration technique on battery electrodes, J. Electrochem. Soc. 164 (2017) A3925, https://doi.org/10.1149/2.1591714jes.
[5] A.V. Churikov, A.V. Ivanishchev, I.A. Ivanishcheva, V.O. Sycheva, N.R. Khasanova, E.V. Antipov, Determination of lithium diffusion coefficient in LiFePO4 electrode by galvanostatic and potentiostatic intermittent titration techniques, Electrochim. Acta 55 (2010) 2939–2950, https://doi.org/10.1016/j.electacta.2009.12.079.
[6] E. Markevich, M.D. Levi, D. Aurbach, Comparison between potentiostatic and galvanostatic intermittent titration techniques for determination of chemical diffusion coefficients in ion-insertion electrodes, J. Electroanal. Chem. 580 (2005) 231–237, https://doi.org/10.1016/j.jelechem.2005.03.030.
[7] J. Li, F. Yang, X. Xiao, M.W. Verbrugge, Y.-T. Cheng, Potentiostatic intermittent titration technique (PITT) for spherical particles with finite interfacial kinetics, Electrochim. Acta 75 (2012) 56–61, https://doi.org/10.1016/j.electacta.2012.04.050.
[8] W. Weppner, R.A. Huggins, Electrochemical investigation of the chemical diffusion, partial ionic conductivities, and other kinetic parameters in Li3Sb and Li3Bi, J. Solid State Chem. 22 (1977) 297–308, https://doi.org/10.1016/0022-4596(77)90006-8.
[9] W. Weppner, R.A. Huggins, Electrochemical methods for determining kinetic properties of solids, Annu. Rev. Mater. Sci. 8 (1978) 269–311, https://doi.org/10.1146/annurev.ms.08.080178.001413.
[10] M.D. Levi, D. Aurbach, The application of electroanalytical methods to the analysis of phase transitions during intercalation of ions into electrodes, J. Solid State Electrochem. 11 (2007) 1031–1042, https://doi.org/10.1007/s10008-007-0264-x.
[11] G. Hasegawa, N. Kuwata, Y. Tanaka, T. Miyazaki, N. Ishigaki, K. Takada, J. Kawamura, Tracer diffusion coefficients of Li + ions in c -axis oriented Li x CoO 2 thin films measured by secondary ion mass spectrometry, Phys. Chem. Chem. Phys. (2021), https://doi.org/10.1039/D0CP04598E.
[12] D.W. Dees, S. Kawauchi, D.P. Abraham, J. Prakash, Analysis of the galvanostatic intermittent titration technique (GITT) as applied to a lithium-ion porous electrode, J. Power Sources 189 (2009) 263–268, https://doi.org/10.1016/j.jpowsour.2008.09.045.
[13] A. Verma, K. Smith, S. Santhanagopalan, D. Abraham, K.P. Yao, P.P. Mukherjee, Galvanostatic intermittent titration and performance based analysis of LiNi0.5Co0.2Mn0.3O2 cathode, J. Electrochem. Soc. 164 (2017) A3380, https://doi.org/10.1149/2.1701713jes.
[14] H. Yang, H.J. Bang, J. Prakash, Evaluation of electrochemical interface area and lithium diffusion coefficient for a composite graphite anode, J. Electrochem. Soc. 151 (2004) A1247, https://doi.org/10.1149/1.1763139.
[15] A. Nickol, T. Schied, C. Heubner, M. Schneider, A. Michaelis, M. Bobeth, G. Cuniberti, GITT analysis of lithium insertion cathodes for determining the lithium diffusion coefficient at low temperature: challenges and pitfalls, J. Electrochem. Soc. 167 (2020), 090546, https://doi.org/10.1149/1945-7111/ab9404.
[16] M.W. Verbrugge, B.J. Koch, Electrochemistry of intercalation materials charge-transfer reaction and intercalate diffusion in porous electrodes, J. Electrochem. Soc. 146 (1999) 833, https://doi.org/10.1149/1.1391689.
[17] K.E. Thomas, J. Newman, R.M. Darling, Mathematical modeling of lithium batteries, in: W.A. van Schalkwijk, B. Scrosati (Eds.), Advances in Lithium-Ion Batteries, Springer US, Boston, MA, 2002, pp. 345–392, https://doi.org/10.1007/0-306-47508-1_13.
[18] Y. Ye, Y. Shi, N. Cai, J. Lee, X. He, Electro-thermal modeling and experimental validation for lithium ion battery, J. Power Sources 199 (2012) 227–238, https://doi.org/10.1016/j.jpowsour.2011.10.027.
[19] D.M. Bernardi, J.-Y. Go, Analysis of pulse and relaxation behavior in lithium-ion batteries, J. Power Sources 196 (2011) 412–427, https://doi.org/10.1016/j.jpowsour.2010.06.107.
[20] V. Sulzer, S.G. Marquis, R. Timms, M. Robinson, S.J. Chapman, Python Battery Mathematical Modelling (PyBaMM), ECSarXiv, 2020, https://doi.org/10.1149/osf.io/67ckj.
[21] EU H2020 Program, Naiades, Sodium Ion Batteries, 2020. http://www.naiades.eu/. (Accessed 29 August 2017).
[22] Naiades | Sodium ion batteries, (n.d.). https://www.naiades.eu/(accessed April 15, 2020).
[23] R. Dugas, B. Zhang, P. Rozier, J.M. Tarascon, Optimization of Na-ion battery systems based on polyanionic or layered positive electrodes and carbon anodes, J. Electrochem. Soc. 163 (2016) A867–A874, https://doi.org/10.1149/2.0051605jes.
[24] H.S. Carslaw, J.C. Jaeger, Conduction of Heat in Solids, Oxford Science Publications, Oxford, England, 1959.
[25] K. Chayambuka, G. Mulder, D.L. Danilov, P.H.L. Notten, A hybrid backward euler control volume method to solve the concentration-dependent solid-state diffusion problem in battery modeling, J. Appl. Math. Phys. 8 (2020) 1066–1080, https://doi.org/10.4236/jamp.2020.86083.
[26] K.L. Gering, Prediction of electrolyte viscosity for aqueous and non-aqueous systems: results from a molecular model based on ion solvation and a chemical physics framework, Electrochim. Acta 51 (2006) 3125–3138, https://doi.org/10.1016/j.electacta.2005.09.011.
[27] J. Lim, Y. Li, D.H. Alsem, H. So, S.C. Lee, P. Bai, D.A. Cogswell, X. Liu, N. Jin, Y. Yu, N.J. Salmon, D.A. Shapiro, M.Z. Bazant, T. Tyliszczak, W.C. Chueh, Origin and hysteresis of lithium compositional spatiodynamics within battery primary particles, Science 353 (2016) 566–571, https://doi.org/10.1126/science.aaf4914.
[28] R.B. Smith, E. Khoo, M.Z. Bazant, Intercalation kinetics in multiphase-layered materials, J. Phys. Chem. C 121 (2017) 12505–12523, https://doi.org/10.1021/acs.jpcc.7b00185.
[29] A. Funabiki, M. Inaba, T. Abe, Z. Ogumi, Stage transformation of lithium-graphite intercalation compounds caused by electrochemical lithium intercalation, J. Electrochem. Soc. 146 (1999) 2443, https://doi.org/10.1149/1.1391953.
[30] B.C. Han, A. Van der Ven, D. Morgan, G. Ceder, Electrochemical modeling of intercalation processes with phase field models, Electrochim. Acta 49 (2004) 4691–4699, https://doi.org/10.1016/j.electacta.2004.05.024.
[31] H.-C. Shin, S.-I. Pyun, The kinetics of lithium transport through Li1−δCoO2 by theoretical analysis of current transient, Electrochim. Acta 45 (1999) 489–501, https://doi.org/10.1016/S0013-4686(99)00270-4.
[32] Z. Liu, Y.-Y. Hu, M.T. Dunstan, H. Huo, X. Hao, H. Zou, G. Zhong, Y. Yang, C.P. Grey, Local structure and dynamics in the Na ion battery positive electrode material Na3V2(PO4)2F3, Chem. Mater. 26 (2014) 2513–2521, https://doi.org/10.1021/cm403728w.
[33] J. Kaspar, M. Graczyk-Zajac, R. Riedel, Determination of the chemical diffusion coefficient of Li-ions in carbon-rich silicon oxycarbide anodes by electro-analytical methods, Electrochim. Acta 115 (2014) 665–670, https://doi.org/10.1016/j.electacta.2013.10.184.